This document is the accepted manuscript version of the following article:
Sun, Q., Mateo, L. M., Robles, R., Ruffieux, P., Lorente, N., Bottari, G., Torres, T., & Fasel, R. (2020). Inducing open-shell character in porphyrins through surface-assisted phenalenyl π-extension. Journal of the American Chemical Society.
https://doi.org/10.1021/jacs.0c07781

Inducing Open-shell Character in Porphyrins through Surface-assisted Phenalenyl π-Extension

Qiang Sun,[⊥,¶] Luis M. Mateo,[†,‡,¶] Roberto Robles,[∥,¶] Pascal Ruffieux,[⊥] Nicolas Lorente,*[,∥,○] Giovanni Bottari,*[,†,‡,§] Tomás Torres*[,†,‡,§] and Roman Fasel*[,⊥,+]

[⊥]nanotech@surfaces Laboratory, Empa-Swiss Federal Laboratories for Materials Science and Technology, 8600 Dübendorf, Switzerland

[†]Departamento de Química Orgánica, Universidad Autónoma de Madrid, 28049 Madrid, Spain

[‡]IMDEA-Nanociencia, Campus de Cantoblanco, 28049 Madrid, Spain

[∥]Centro de Física de Materiales CFM/MPC (CSIC-UPV/EHU), Paseo de Manuel de Lardizabal 5, 20018 Donostia-San Sebastián, Spain

[○]Donostia International Physics Center (DIPC), 20018 Donostia-San Sebastián, Spain

[§]Institute for Advanced Research in Chemical Sciences (IAdChem), Universidad Autónoma de Madrid, 28049 Madrid, Spain

[+]Department of Chemistry and Biochemistry, University of Bern, 3012 Bern, Switzerland

ABSTRACT: Organic open-shell compounds are extraordinarily attractive materials for their use in molecular spintronics thanks to their long spin-relaxation times and structural flexibility. Porphyrins (Pors) have widely been used as molecular platforms to craft persistent open-shell structures through solution-based redox chemistry. However, very few examples of inherently open-shell Pors have been reported, which are typically obtained through the fusion of non-Kekulé polyaromatic hydrocarbon moieties to the Por core. The inherent instability and low solubility of these radical species, however, requires the use of bulky substituents and multi-step synthetic approaches. On-surface synthesis has emerged as a powerful tool to overcome such limitations, giving access to structures that cannot be obtained through classical methods. Herein, we present a simple and straightforward method for the on-surface synthesis of phenalenyl-fused Pors using readily available molecular precursors. In a systematic study, we examine the structural and electronic properties of three surface-supported Pors, bearing zero, two (**PorA$_2$**) and four (**PorA$_4$**) *meso*-fused phenalenyl moieties. Through atomically resolved real-space imaging by scanning probe microscopy and high-resolution scanning tunneling spectroscopy combined with density functional theory (DFT) calculations, we unambiguously demonstrate a triplet ground state for **PorA$_2$** and a charge transfer induced open-shell character for the intrinsically closed-shell **PorA$_4$**.

INTRODUCTION

Porphyrins (Pors), tetrapyrrolic macrocycles with a planar structure and an aromatic circuit of 18 π-electrons, are heterocycles showing high thermal stability,[1] rich coordination chemistry,[2] tunable redox features,[3] and excellent photophysical properties.[4] Their unique features make these chromophores prime candidates for a wide range of applications ranging from materials science,[5] catalysis,[6] photovoltaics,[7-10] or medicine,[11] to mention a few.

Remarkably, many of these properties can be precisely tuned through chemical modifications, such as the complexation of metal ions[2] or the modification of number and nature of the peripheral substituents.[4] Among such structural modifications, the π-extension of the Por core is particularly appealing, since it leads to compounds with a strong near-infrared (NIR) absorption, stemming from a small highest occupied molecular orbital (HOMO)-lowest unoccupied molecular orbital (LUMO) gap.[12] Such π-extended Pors can be obtained either by attaching other aromatic units to the macrocycle *via* conjugative linkers[9,13-16] or through the *meso*,*β*-fusion of aromatic units *via* intramolecular oxidative coupling.[17-24] Using the latter synthetic strategy, a wide range of π-extended Pors has been reported, showing, in some cases, absorptions reaching far into the NIR region (*i.e.*, 1417 nm) and optical HOMO-LUMO gaps as low as 0.61 eV.[25] However, the vast majority of these systems presents a closed-shell character,[26] while only few examples of open-shell analogues have been reported.[27,28] Organic open-shell structures are extraordinarily attractive materials in spintronics, presenting longer spin-relaxation times and easier tunability than inorganic materials.[27,29-31] Along this line, Osuka and co-workers reported the preparation of several inherent and persistent Por-based radicals using rational molecular design and, in most examples, redox chemistry.[28] These radicals are either

charged (anions/cations) or neutral with the unpaired electron poorly delocalized over the macrocycle.

Over the past years, the preparation and study of π-extended Pors with highly delocalized radicals has, therefore, gathered significant attention. For this purpose, an interesting yet poorly explored strategy consists in the fusion of inherently radical polyaromatic hydrocarbons (PAHs) to the macrocycle.[32-34] Among these PAHs, non-Kekulé structures like phenalenyl – its smallest member – have been widely used as a building block to generate radicaloid and biradicaloid structures with remarkable thermodynamic stability.[27,29,35-40] However, the synthetic access to phenalenyl-based structures is often hampered by multistep synthesis, low yields, and poorly soluble intermediates and products. Moreover, the inherently low HOMO-LUMO gap of phenalenyl leads to stability issues, such that the characterization of these species needs to be carried out in degassed solutions or through *in-situ* generation of the radical species.[32]

On-surface synthesis stands as a promising tool to prepare open-shell PAH systems, offering significant advantages over the more classical "wet" synthesis. The employed ultra-high vacuum (UHV) conditions and the atomically clean, catalytic surfaces used, provide the ideal playground for both synthesis and characterization of structures that are hardly accessible through solution-based methods.[41-50] Indeed, recently, elusive PAHs or nanographenes with open-shell characters such as Clar's goblet and triangulenes have been successfully realized through on-surface synthesis.[47,51-54] The on-surface chemistry of Pors and related porphyrinoids has emerged in the past decades,[55,56] focusing mainly on model systems like porphines,[57,58] tetraphenylPors,[59-61] and derivatives thereof.[62-64] On-surface fabrication of π-extended Pors by fusing the macrocycle with PAHs has only recently been reported.[58,65-67] However, the few reported examples involve hybrids of Por with nanographenes, not focusing on the possible open-shell character of the π-system.

Herein, we present the on-surface synthesis and characterization of three Zn(II)Pors, namely **PorA$_0$**, **PorA$_2$**, and **PorA$_4$**, with zero, two, and four *meso*,*β*,*β* triply-fused phenalenyl moieties, respectively. While **PorA$_0$** was prepared by "wet" synthesis, the two- and four-fold phenalenyl-fused Por derivatives **PorA$_2$** and **PorA$_4$** were fabricated through a surface-assisted cyclodehydrogenation reaction[68] from *meso*-2,6-dimethylphenyl (dmp) substituted precursors **Por(dmp)$_2$** and **Por(dmp)$_4$**, respectively. This study reveals the electronic impact of the phenalenyl substituents fused to the Por macrocycle, leading to the open-shell character for **PorA$_2$**, which is demonstrated by DFT calculations and resonance structure analysis. Further proof of the open-shell character of **PorA$_2$** is provided by the coexistence of singly and doubly *β*-hydrogenated Pors with the intact **PorA$_2$**. Furthermore, we have explored the electronic properties of all three fabricated molecules by STS. For **PorA$_2$**, an open-shell triplet ground state is experimentally demonstrated by inelastic spin excitation and Kondo scattering at low energies. For **PorA$_4$**, DFT calculations and resonance structure analysis both predict a closed-shell electronic structure. Interestingly, charge transfer to the underlying surface gives rise to induced open-shell character to the intrinsically closed-shell **PorA$_4$**, as reflected by a characteristic Kondo resonance.

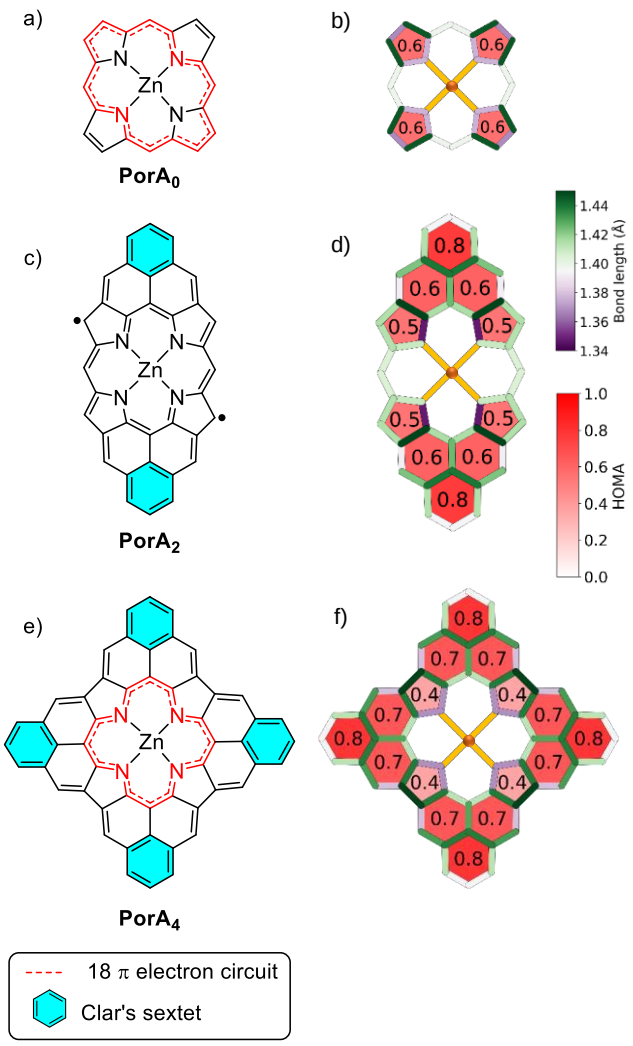

Figure 1. Molecular structures of a) **PorA$_0$**, c) **PorA$_2$**, and e) **PorA$_4$**. In c,e), turquoise hexagons identify Clar's sextets, whereas in a,e), red dashed lines indicate a 18 π-electron circuit. HOMA and bond length analysis of b) **PorA$_0$**, d) **PorA$_2$**, and f) **PorA$_4$**. The scale bars for bond length and HOMA apply to b), d) and f). Zn-N bonds do not correlate with the color scale and have been colored in orange.

Results and Discussion

Synthesis of PorA$_0$, and precursors of PorA$_2$ and PorA$_4$

D_{4h}-symmetric **H$_2$PorA$_0$** and **H$_2$Por(dmp)$_4$** were prepared by condensing pyrrole with formaldehyde or 2,6-dimethylbenzalehyde, respectively, under classical Lindsey conditions (Scheme 1a,c).[69] While the condensation reaction involving 2,6-dimethylbenzaldehyde afforded **H$_2$Por(dmp)$_4$** in 15% yield, the low reactivity and solubility of formaldehyde limited the yield of **H$_2$PorA$_0$** (*i.e.*, 1.5%) with a considerable amount of polypyrrolic tar obtained as side-product. D_{2h}-symmetric **H$_2$Por(dmp)$_2$** was prepared in 27% yield by condensing *meso*-H-dipyrromethane with 2,6-dimethylbenzaldehyde under standard Lindsey conditions (Scheme 1b). Subsequent metalation of **H$_2$PorA$_0$**, **H$_2$Por(dmp)$_2$**, and **H$_2$Por(dmp)$_4$** with Zn(OAc)$_2$ in reflux-

ing THF afforded the corresponding zinc metalated derivatives **PorA$_0$**, **Por(dmp)$_2$**, and **Por(dmp)$_4$**, respectively, in excellent yields. **PorA$_0$**, **Por(dmp)$_2$**, and **Por(dmp)$_4$**, as well as their precursors, were fully characterized by a wide range of spectroscopic and spectrometric techniques (see Supporting Information).

Scheme 1. Synthetic route to the preparation of a) PorA$_0$, b) PorA$_2$, and c) PorA$_4$.[a]

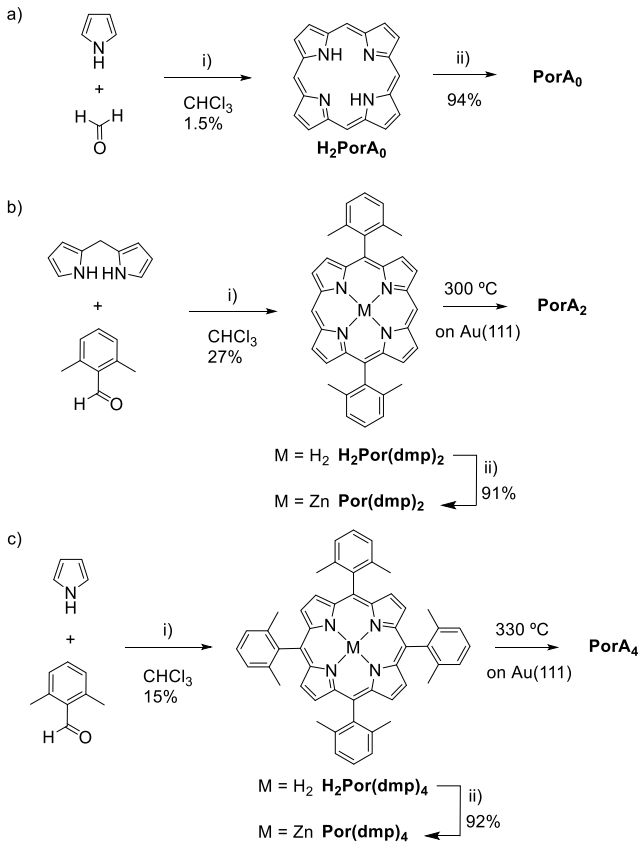

[a] Reagents and conditions: i) 1) $BF_3O(Et)_2$, r.t., 2) DDQ, reflux, 3) NEt_3, r.t. ii) $Zn(OAc)_2$, THF, reflux; DDQ = 2,3-dichloro-5,6-dicyano-1,4-benzoquinone.

On-surface Synthesis and Characterization of PorA$_0$, PorA$_2$, and PorA$_4$.

PorA$_0$ was deposited on Au(111) at room temperature and examined by STM imaging after cool down to 4.5 K, yielding samples of high purity and homogeneity (Figure 2a). On the other hand, samples with deposited precursors **Por(dmp)$_2$** and **Por(dmp)$_4$** were annealed above 300 ° C to promote the surface-assisted cyclodehydrogenation between the methyl groups and the macrocycle, giving **PorA$_2$** and **PorA$_4$**, respectively.[66] The corresponding large-scale STM images of **PorA$_2$** and **PorA$_4$** confirm the presence of individual molecules, but also reveal several side-products, which are tentatively identified as covalently-linked dimers and trimers (Figure 2d,g). High-resolution STM images (Figure 2b,e,h) reveal fully planarized structures with the expected symmetry (*i.e.*, D_{4h} for **PorA$_0$** and **PorA$_4$**, and D_{2h} for **PorA$_2$**), suggesting the successful formation of the target structures. Finally, the molecular structures were unambiguously confirmed by bond-resolved nc-AFM imaging (Figure 2c,f,i).

In a first step, the potential open-shell character of **PorA$_0$**, **PorA$_2$**, and **PorA$_4$** was evaluated based on their resonance structures. **PorA$_0$** presents a conjugated circuit of 18 π-electrons, fulfilling Hückel's rule (Figure 1a), and its predicted electronic character is closed-shell. However, the fusion of two and four phenalenyls to the Por core leading to **PorA$_2$** and **PorA$_4$**, respectively, gives rise to non-Kekulé resonance structures (Figure 1c,e and Figures S4.1 and S4.2). In the case of **PorA$_2$**, several resonance structures, all of which are non-Kekulé, can be drawn (Figure S4.1). Among those, the ones which show the maximum number of Clar's sextets (*i.e.*, 2) and minimum number of unpaired electrons (*i.e.*, 2) – as the one drawn in Figure 1c (*vide infra*) – can be expected to contribute most to the ground state electronic structure. It is worth to notice that none of the relevant resonance structures preserves the inner Por 18 π-electron aromatic circuit. For **PorA$_4$**, a closed-shell Kekulé structure with four Clar's sextets on the phenalenyls and an 18 π-electron circuit on the central macrocycle can be drawn (Figure 1e). In addition, several non-Kekulé structures can be proposed (Figure S4.2), one of which minimizes the number of radicals (*i.e.*, 2) while maintaining the four Clar's sextets (Figure S4.2b). To obtain further insights, harmonic oscillator model of aromaticity (HOMA)[70,71] analysis has been performed on DFT optimized **PorA$_2$** and **PorA$_4$** in the gas phase. These studies show excellent agreement with the proposed resonance structures, assigning high and low degree of benzenoid character to the outermost six-membered rings and the pyrrolic units, respectively (Figure 1d,f). Furthermore, gas-phase DFT calculations at the B3LYP level show that, for **PorA$_2$**, the open-shell electronic configuration is 0.46 eV more stable than the closed-shell one. On the other hand, in the case of **PorA$_4$**, the closed-shell electronic configuration is 0.21 eV more stable than the open-shell one by theory.

Particular attention was therefore paid to **PorA$_2$**, aimed at confirming its predicted open-shell character. Surprisingly, after a close inspection of the reaction products by taking a number of high-resolution nc-AFM images, we found that there were two other species besides **PorA$_2$** (Figure 3, panel iii) which were almost indiscernible from normal topographic STM images (Figure 3, panel ii). One species features two bright protrusions at opposite *β*-sites of the macrocycle in nc-AFM images (Figure 3a, panel iii), while another only features one protrusion at a *β*-site (Figure 3b, panel iii). Since constant-height nc-AFM imaging is very sensitive to the apparent height of the underlying structures, each bright protrusion suggests a doubly hydrogenated sp^3 hybridized carbon (CH_2) as also observed in other open-shell nanographene systems.[47,48] Remarkably, these hydrogenated *β* positions correspond with the sites of the unpaired electrons in the proposed resonance structure of **PorA$_2$** (Figure 1c).

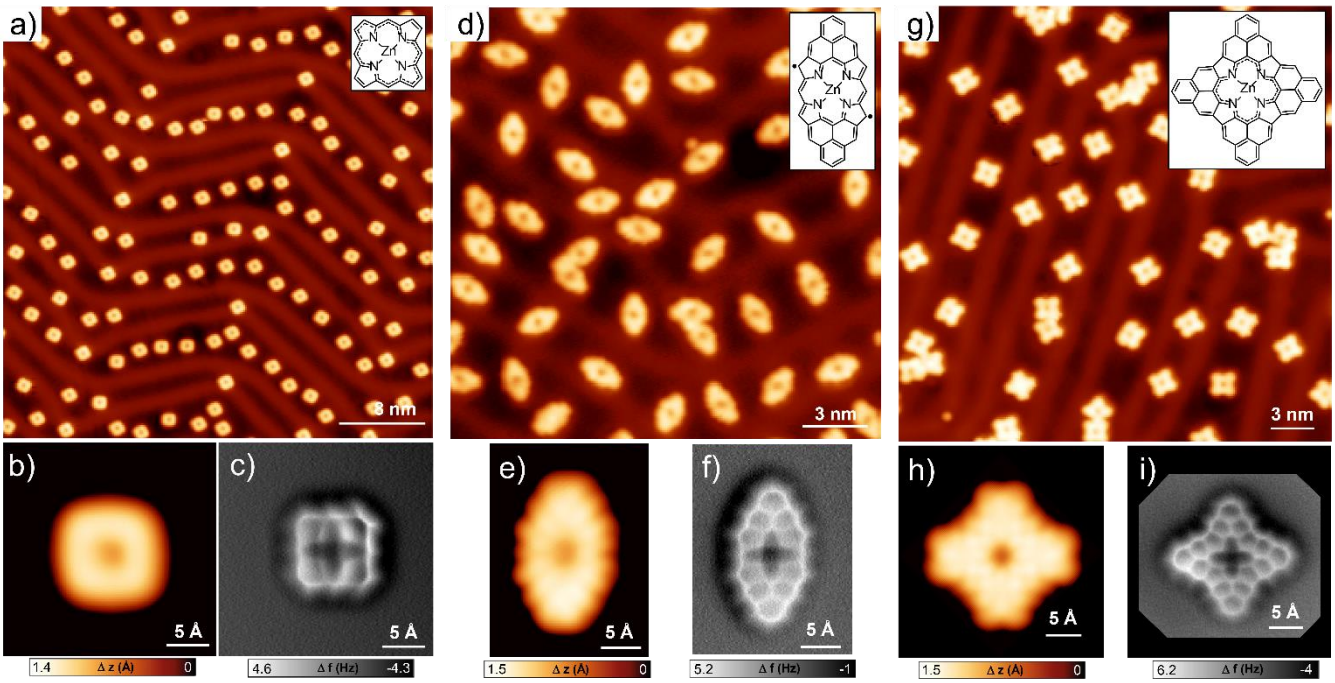

Figure 2. a) Large-scale STM image of **PorA$_0$** (chemical structure in the inset) as-deposited on Au(111) at room temperature (V_s = –0.5 V, I_t = 50 pA). b) Close-up STM (V_s = –0.6 V, I_t = 400 pA) and c) constant-height nc-AFM (V_s = –0.001 V) images of **PorA$_0$**. d) Large-scale STM image of **PorA$_2$** (chemical structure in the inset) obtained upon annealing of **Por(dmp)$_2$** at 300 °C on Au(111) (V_s = –0.2 V, I_t = 50 pA). e) Close-up STM (V_s = –0.06 V, I_t = 150 pA) and f) constant-height nc-AFM (V_s = –0.005 V) images of **PorA$_2$**. g) Large-scale STM image of **PorA$_4$** (chemical structure in the inset) obtained upon annealing of **Por(dmp)$_4$** at 330 °C on Au(111) (V_s = –0.2 V, I_t = 50 pA). h) Close-up STM (V_s = –0.1 V, I_t = 150 pA) and i) constant-height nc-AFM (V_s = –0.005 V) images of **PorA$_4$**.

STM induced atomic manipulation can be employed to selectively break one C-H bond and transform C(sp^3)H$_2$ into C(sp^2)H, as the C-H bond-dissociation energy is lower in CH$_2$ than in CH.[47,48] To further elucidate the chemical structures of the hydrogen passivated species, we applied a corresponding STM manipulation protocol. The tip was initially positioned above a bright protrusion (CH$_2$) of a di-hydrogenated **PorA$_2$(H$_2$)** with a typical STM setpoint of V = –0.1 V and I = 10 pA (Figure 3a). The tip was thereafter retracted by 4 Å to limit the tunneling current at the open-feedback loop. Then the voltage bias was gradually ramped up to 3.4 eV until an abrupt change of the tunneling current occurred, indicating a manipulation event. The resulting structure was imaged by both high-resolution STM and nc-AFM, revealing the formation of the mono-hydrogenated **PorA$_2$(H)** species (Figure 3b). Repeating the same protocol, **PorA$_2$(H)** can be further transformed into **PorA$_2$** (Figure 3c). The success rate of such atomic manipulation is as high as 90% without disrupting the molecular structure. These manipulation experiments suggest that **PorA$_2$(H)** and **PorA$_2$(H$_2$)** are derived from initially formed **PorA$_2$** through its passivation with H$_2$ from the cyclodehydrogenation process. DFT calculations on the surface show that passivating **PorA$_2$** is favorable by 0.79 eV per H, in agreement with the experimental observations. The presence of **PorA$_2$(H)** and **PorA$_2$(H$_2$)** implies a high reactivity of **PorA$_2$**, indicating a certain radical character, in line with the predicted open-shell structure (Figure 1b).

An important and direct fingerprint of molecules with open-shell character is the presence of low-energy spectral features in the differential conductance (dI/dV) spectroscopy revealing inelastic spin excitations and/or a Kondo resonance.[72] Thus, dI/dV spectra were taken on **PorA$_2$** with a focus on the low bias range (Figure 3d). Interestingly, we observed characteristic conductance steps symmetrically located around the Fermi level, along with a zero-bias peak. The step-like conductance increase can be associated with the inelastic excitation between the ferromagnetic (triplet) ground state and an antiferromagnetic (singlet) excited state, while the zero-bias peak is usually related to the many-body Kondo state arising from the screening of a localized spin by itinerant electrons from the metal surface.[73] However, unlike spin excitation spectra for organic systems with singlet ground states,[51,74] the coexistence of conductance steps and a zero-bias peak points toward a triplet S = 1 ground state.[75] The low-energy dI/dV spectrum can be nicely fit by a dynamical scattering model developed by M. Ternes,[72] in which we constructed a S = 1 system with two ferromagnetically exchange-coupled spins. An exchange coupling energy J = 19.4 meV was derived from the fit. Our DFT calculations on the surface and in gas phase both predict a ferromagnetic ground state, with a 25 meV higher antiferromagnetic state (gas phase). Note the obtained value of J is comparable to the exchange coupling energy of open-shell nanographenes on surface with few tens of meV.[51,53] Moreover, we found that inclusion of a non-zero Kondo scattering parameter $J\rho_s$ is crucial to reproduce both the cusp above the excitation energy and the zero-bias peak in the spectrum, with a value of –0.14 determined from the fit. Here, J is the exchange coupling strength between the magnetic impurity and the substrate, and ρ_s is the free electron density. The Kondo temperature is directly related to $J\rho_s$, as $T_K \propto \exp(-1/\rho J)$. In Figure 3e, we show the spin excitation maps of **PorA$_2$** obtained by constant height STS at $\pm$ 22 mV,

which agree with the spin density map of the ferromagnetic (triplet) ground state. The nodal pattern of the experimental maps is different from the one of the simulated spin density map because the p-wave nature of the CO-functionalized tip was not taken into account in the simulations.[76] The effect of the substrate will be discussed by our detailed DFT calculations in the following context.

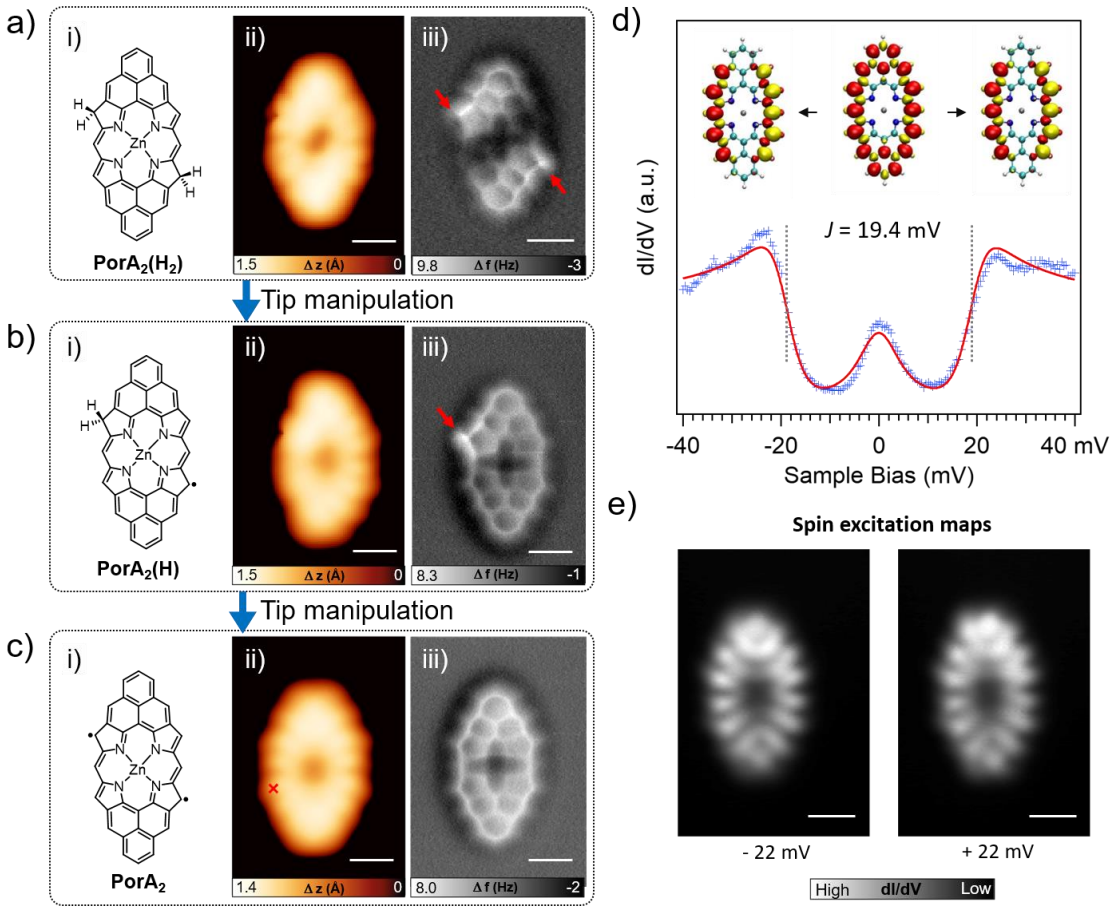

Figure 3. a) i): Chemical structure of **PorA$_2$(H$_2$)**; ii): high-resolution STM (V_s = –0.04 V, I_t = 100 pA) and iii) nc-AFM (V_s = –0.005 V) images where the doubly hydrogenated sites are indicated by arrows. b) i): Chemical structure of **PorA$_2$(H)**; ii) its high-resolution STM (V_s = –0.06 V, I_t = 200 pA) and iii) nc-AFM (V_s = –0.005 V) images where the doubly hydrogenated site is indicated by an arrow. c) i): Chemical structure of **PorA$_2$**; ii): its high-resolution STM (V_s = –0.06 V, I_t = 200 pA) and iii) nc-AFM (V_s = –0.005 V) images. The stepwise transformation of a) **PorA$_2$(H$_2$)** to b) **PorA$_2$(H)** to c) **PorA$_2$** can be achieved by STM tip induced hydrogen abstraction. Scale bar: 5 Å. d) dI/dV spectrum acquired over **PorA$_2$** at the position marked in c) (V_{mod} = 0.8 mV). The data is shown by blue markers, and the solid red line is a fit based on a dynamical scattering model developed by M. Ternes.[68] DFT calculated spin density maps for the ferromagnetic and antiferromagnetic ground states are displayed in the inset, where red and yellow densities denote the spin-up and spin-down contributions, respectively. e) Constant-height STS maps taken at bias voltages of –22 mV and 22 mV (V_{mod} = 4 mV). The spin excitation maps were acquired with a CO-functionalized tip. Scale bar: 5 Å.

The electronic properties of **PorA$_0$**, **PorA$_2$**, and **PorA$_4$** were further investigated by wider bias range differential conductance dI/dV spectroscopy to probe their local density of states (LDOS). The dI/dV spectrum of **PorA$_0$** reveals a wide energy gap around the Fermi level which is enclosed by two broad peaks beyond ±1V (Figure 4a). The energy gap on Au(111), around 2.3 eV derived from the onsets of the peaks, is comparable to the one of tetraphenyl-Por on Au(111),[77] and the corresponding negative and positive ion resonances can accordingly be assigned to the Por HOMO and LUMO, respectively. dI/dV maps were acquired at the onset energies of the two peaks (Figure 4b), showing the spatially resolved HOMO (–1.0 V) and LUMO (1.3 V) orbitals. DFT calculations of the **PorA$_0$** on Au(111) were performed to give further insights (Figure S2.1). Both the experimental dI/dV spectrum and maps are in good agreement with the DFT computed projected density of states (PDOS) of the surface-supported **PorA$_0$** (Figure 4c) and its corresponding simulated dI/dV maps (Figure 4d), respectively. The fusion of two phenalenyls to the Por core in **PorA$_2$** significantly alters the molecular energy level structure, and the resulting dI/dV spectrum exhibits three broad peaks in the probed energy range (Figure 4e). Spin-polarized DFT calculations were performed to elucidate the electronic structure of **PorA$_2$** on Au(111) (Figure S2.2). They reveal a rather complicated energy level renormalization for this open-shell molecule (Figure 4g). The DOS projected on the frontier molecular orbitals shows that the gas-phase HOMO of **PorA$_2$** gets empty for the spin-up electrons upon adsorption on Au(111), which is also reflected in the calculated charge transfer of −0.73 electrons. We note that a direct comparison between the dI/dV maps of **PorA$_2$** acquired at different

bias voltages with the DFT computed dI/dV maps is difficult due to the underestimation of the HOMO-LUMO gap inherent to DFT. In order to ease the comparison, we have used the cation of **PorA$_2$** (with 1 electron being removed) in the gas phase as a model system of the surface supported molecule. Calculations of the gas phase cation at the B3LYP level of theory combined with the results on the surface obtained at the PBE level (see discussions in Figure S2.2 and S2.3) allow us to assign the peak at 0.6 V in Figure 4e to the empty molecular spin-up HOMO, while the peak starting from 1.3 V is assigned to the spin-down LUMO and LUMO+1 (Figure 4f-h) and the broad peak at the negative side from –0.4 V is assigned to the spin-up HOMO-1. It is important to note that, despite the charge transfer of **PorA$_2$** to the Au(111) substrate, a ferromagnetic ground state is also predicted by DFT (Figure S2.3).

Turning to **PorA$_4$**, its dI/dV spectrum shows a broad density of states from 0.5 V to 1.2 V and a sharp peak around 1.9 V (Figure 4i). Our DFT calculations indicate a charge transfer of –1.11 electrons from the molecule to the surface, which agrees with the HOMO getting empty in the DOS projected on molecular orbitals (Figure S2.4 and Figure 4k). We can therefore assign the broad feature in the dI/dV spectrum to the emptied spin-down HOMO, the doubly degenerate LUMO, and the LUMO+1. The sharp peak at 1.9 V is assigned to the LUMO+2. This assignment of molecular orbitals is corroborated by the excellent match between experimental and theoretical maps (Figure 4j and 4l, respectively), which further confirms the DFT prediction of a sizable electron transfer from the Por to the substrate.

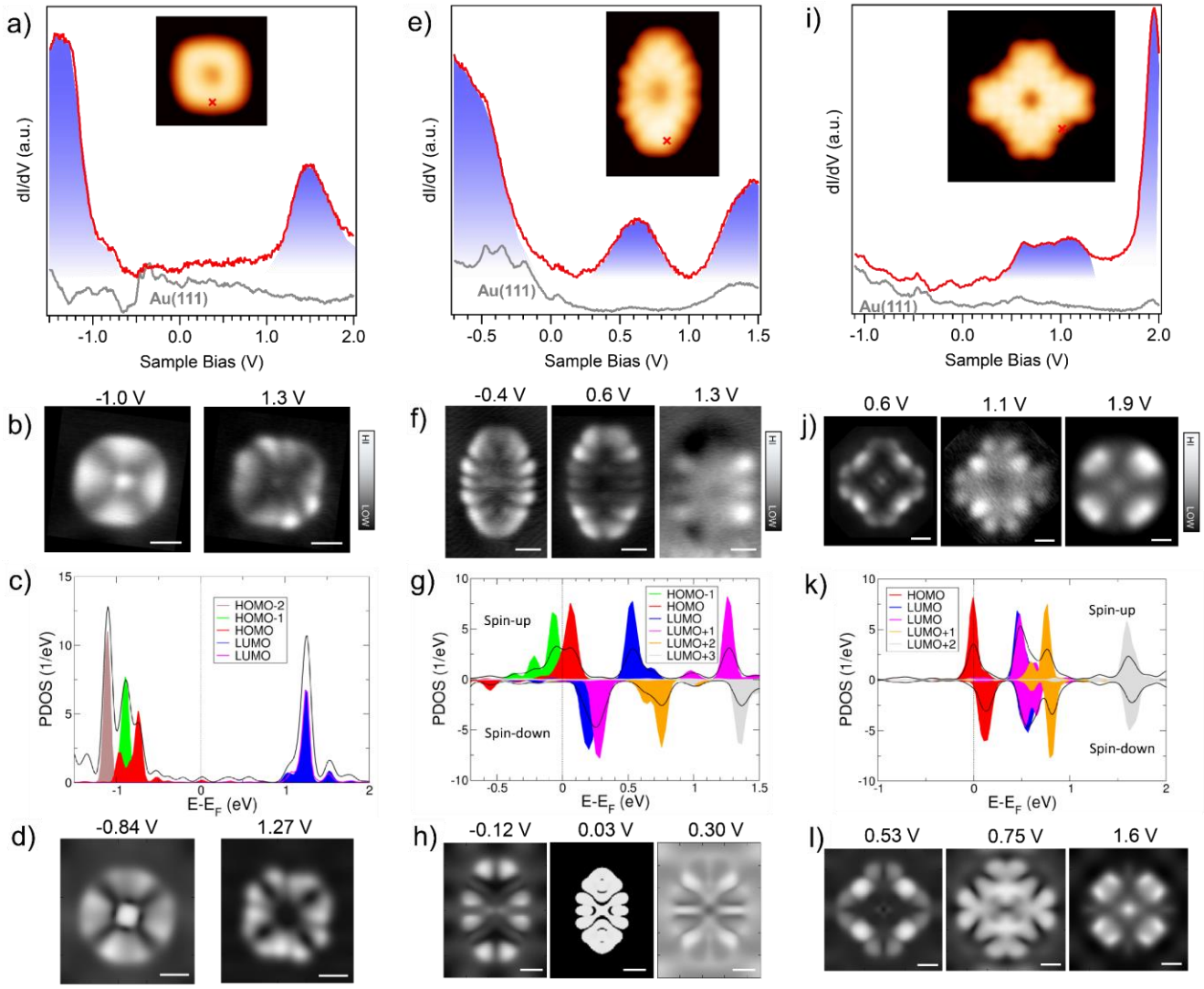

Figure 4. a,e,i) Wide bias range STS spectrum of **PorA$_0$**, **PorA$_2$** and **PorA$_4$**, respectively. The corresponding STM images and the acquisition position of the STS spectra are shown in the inset; b,f,j) constant-current STS maps recorded at the energies of the prominent peaks; c,g,k) DFT computed PDOS (black curve) on the surface-supported **PorA$_0$**, **PorA$_2$** and **PorA$_4$**, respectively, where the colored areas indicate the PDOS on its corresponding gas-phase molecular orbitals (gas phase molecular orbitals indicated in Figure S2); d) simulated dI/dV maps matching the experimental ones in (b); h) simulated dI/dV maps matching the experimental ones in (f); l) simulated dI/dV maps matching the experimental ones in (j). Scale bars in b,d,f,h,j,l): 5 Å.

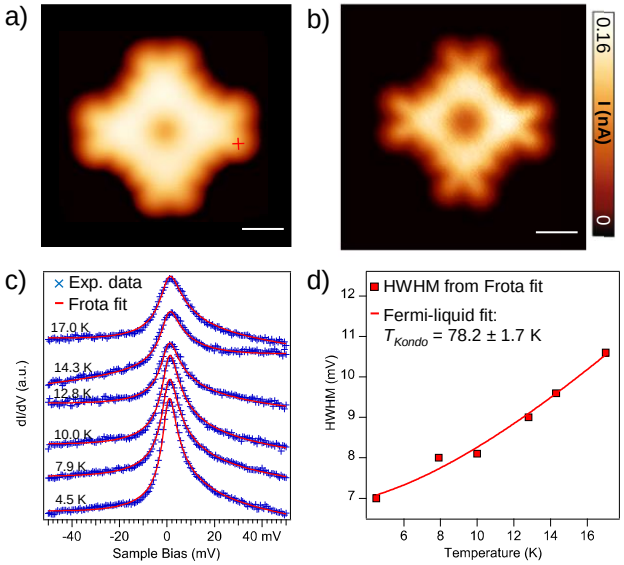

Figure 5. a) Low-bias STM topography (V_s = − 0.05 V, I_t = 450 pA) and b) constant-height STM image (V_s = 5 mV) of **PorA$_4$** on Au(111). Scale bar: 5 Å. c) Temperature evolution of the STS spectra for **PorA$_4$** with the experimental data fit by the Frota function. The acquisition position of STS spectra is marked in a) (V_{mod} = 0.8 mV). d) Extracted half width at half maximum (HWHM) of the Kondo resonance as a function of temperature, which is fit using the Fermi-liquid model to determine the Kondo temperature.

The charging of a closed-shell molecule as a consequence of molecule-to-surface charge transfer could give rise to unpaired electrons on the molecule and induce a magnetic moment.[78] Indeed, we observed a pronounced zero-bias resonance in low-energy dI/dV spectra acquired on **PorA$_4$** (Figure 5c). The resonance can be fit by a Frota function describing a Kondo resonance, from which the resonance width (half width at half maximum, HWHM) can be abstracted. The HWHM of the resonance exhibits a characteristic temperature dependent broadening following the Fermi-liquid model, evidencing a Kondo resonance with a Kondo temperature T_K = 78 K extracted from the Fermi-liquid fit (Figure 5d). This unambiguously evidences the presence of an unpaired electron with S=1/2 on the surface supported **PorA$_4$** molecule. The charge-transfer induced magnetic properties of the surface supported **PorA$_4$** agree with the DFT calculations that indicate a charge transfer of −1.11 electrons and a magnetic moment of 0.69 μ_B, compatible with a S=1/2 ground state. Moreover, constant-height current maps around the Kondo peak (V = 5 mV), approximating the Kondo map of **PorA$_4$** on Au(111) (Figure 5b) show a good agreement with the corresponding DFT computed spin density map (Figure S2.5). We note that due to the atomic defects existing in both PorA$_2$ and PorA$_4$ samples, the yields of the defect-free PorA$_2$ and PorA$_4$ are around 15 % and 5%, respectively.

During the reviewing of this manuscript, we became aware of a related work on π-extended porphyrins.[79]

CONCLUSION

We have reported an in-depth study on the effect of phenalenyl π-extension of Pors as an efficient way to induce open-shell character in Pors. For this purpose, three Pors presenting zero (*i.e.*, **PorA$_0$**), two (*i.e.*, **PorA$_2$**), or four (*i.e.*, **PorA$_4$**) phenalenyl moieties fused to the macrocycle were investigated. While **PorA$_0$** was prepared by solution chemistry and deposited as such on Au(111), **PorA$_2$** and **PorA$_4$** were obtained by surface-assisted cyclodehydrogenation from appropriate *meso*-(2,6-dimethylphenyl)-functionalized Por precursors.

The potential open-shell character of these three Pors was evaluated, firstly, by consideration of their resonance structures and by gas-phase DFT calculations. In the case of **PorA$_0$**, only Kekulé resonance structures can be drawn, suggesting a closed-shell character, which is confirmed by DFT. On the other hand, DFT calculations on **PorA$_2$** predict an open-shell character, which is in line with the non-Kekulé resonance structures that can be proposed for this Por. In the case of **PorA$_4$**, DFT calculations and resonance structure analysis both predict a closed-shell character, while some reasonable non-Kekulé resonance structures can also be proposed.

The three surface-supported Pors were characterized by high-resolution STM and atomically resolved nc-AFM imaging. Interestingly, in the case of **PorA$_2$**, the presence of singly and doubly *β*-hydrogenated Por species was also observed, further supporting the hypothesis of a marked open-shell character. Moreover, the doubly hydrogenated Por could be converted into the singly hydrogenated species and the latter into pristine **PorA$_2$** by STM atomic manipulation. Unequivocal evidence for an open-shell character of **PorA$_2$** was obtained from low-bias STS, where we found coexistence of inelastic excitations and a zero-bias peak, suggesting a triplet ground state. Additionally, charge transfer to the surface gives rise to induced open-shell character to the intrinsically closed-shell **PorA$_4$**, which presents a characteristic Kondo resonance. Our results evidence a facile strategy to the formation of open-shell Por molecules, which are promising for future molecular electronics and spintronics.

ASSOCIATED CONTENT

The Supporting Information is available free of charge on the ACS Publications website at DOI:

Synthesis detail of the precursor molecules, experimental and theoretical details, resonance structures for PorA2 and PorA4

AUTHOR INFORMATION

Corresponding Authors

*roman.fasel@empa.ch
*nicolas.lorente@ehu.eus
*tomas.torres@uam.es
*giovanni.bottari@uam.es

Author Contributions

¶Q.S., L.M.M. and R.R. contributed equally to this work.

Notes

The authors declare no competing financial interest.

ACKNOWLEDGMENT

This work was supported by the Swiss National Science Foundation under Grant No. 200020_182015. Financial support from Spanish MICINN (CTQ2017-85393-P) and ERA-NET/European Commission/MINECO (UNIQUE, SOLAR-ERA.NET Cofund 2 N° 008/ PCI2019-111889-2) are acknowledged. IMDEA Nanociencia acknowledges support from the "Severo Ochoa" Programme for Centres of Excellence in R&D (MINECO, Grant SEV2016-0686). R.R. and N.L. are grateful for funding from the EU-FET Open H2020 Mechanics with Molecules project (grant 766864). Q.S. thanks Kristjan Eimre for helping in HOMA analysis.

REFERENCES

(1) Liu, Z.; Yasseri, A. A.; Lindsey, J. S.; Bocian, D. F., Molecular memories that survive silicon device processing and real-world operation, *Science* **2003**, *302*, 1543-1545.

(2) Suijkerbuijk, B. M. J. M.; Klein Gebbink, R. J. M., Merging porphyrins with organometallics: Synthesis and applications, *Angew. Chem. Int. Ed.* **2008**, *47*, 7396-7421.

(3) Boulas, P. L.; Gómez-Kaifer, M.; Echegoyen, L., Electrochemistry of supramolecular systems, *Angew. Chem. Int. Ed.* **1998**, *37*, 216-247.

(4) Mandal, A. K.; Taniguchi, M.; Diers, J. R.; Niedzwiedzki, D. M.; Kirmaier, C.; Lindsey, J. S.; Bocian, D. F.; Holten, D., Photophysical properties and electronic structure of porphyrins bearing zero to four meso-phenyl substituents: New insights into seemingly well understood tetrapyrroles, *J. Phys. Chem. A* **2016**, *120*, 9719-9731.

(5) Jurow, M.; Schuckman, A. E.; Batteas, J. D.; Drain, C. M., Porphyrins as molecular electronic components of functional devices, *Coord. Chem. Rev.* **2010**, *254*, 2297-2310.

(6) Beyene, B. B.; Hung, C.-H., Recent progress on metalloporphyrin-based hydrogen evolution catalysis, *Coord. Chem. Rev.* **2020**, *410*, 213234.

(7) Hasobe, T., Porphyrin-based supramolecular nanoarchitectures for solar energy conversion, *J. Phys. Chem. Lett.* **2013**, *4*, 1771-1780.

(8) Urbani, M.; Grätzel, M.; Nazeeruddin, M. K.; Torres, T., Meso-substituted porphyrins for dye-sensitized solar cells, *Chem. Rev.* **2014**, *114*, 12330-12396.

(9) Mathew, S.; Yella, A.; Gao, P.; Humphry-Baker, R.; Curchod, B. F. E.; Ashari-Astani, N.; Tavernelli, I.; Rothlisberger, U.; Nazeeruddin, M. K.; Grätzel, M., Dye-sensitized solar cells with 13% efficiency achieved through the molecular engineering of porphyrin sensitizers, *Nat. Chem.* **2014**, *6*, 242-247.

(10) Wang, C.-L.; Hu, J.-Y.; Wu, C.-H.; Kuo, H.-H.; Chang, Y.-C.; Lan, Z.-J.; Wu, H.-P.; Wei-Guang Diau, E.; Lin, C.-Y., Highly efficient porphyrin-sensitized solar cells with enhanced light harvesting ability beyond 800 nm and efficiency exceeding 10%, *Energy Environ. Sci.* **2014**, *7*, 1392-1396.

(11) Rajora, M. A.; Lou, J. W. H.; Zheng, G., Advancing porphyrin's biomedical utility via supramolecular chemistry, *Chem. Soc. Rev.* **2017**, *46*, 6433-6469.

(12) Anderson, H. L., Building molecular wires from the colours of life: Conjugated porphyrin oligomers, *Chem. Commun.* **1999**, 2323-2330.

(13) Screen, T. E. O.; Blake, I. M.; Rees, L. H.; Clegg, W.; Borwick, S. J.; Anderson, H. L., Making conjugated connections to porphyrins: A comparison of alkyne, alkene, imine and azo links, *J. Chem. Soc., Perkin Trans. 1* **2002**, 320-329.

(14) Chang, J.-C.; Ma, C.-J.; Lee, G.-H.; Peng, S.-M.; Yeh, C.-Y., Porphyrin–triarylamine conjugates: Strong electronic communication between triarylamine redox centers via the porphyrin dication, *Dalton T* **2005**, 1504-1508.

(15) Zhou, Y.; Ngo, K. T.; Zhang, B.; Feng, Y.; Rochford, J., Synthesis, electronic and photophysical characterization of π-conjugated meso-ferrocenyl-porphyrin fluorescent redox switches, *Organometallics* **2014**, *33*, 7078-7090.

(16) Hadmojo, W. T.; Lee, U.-H.; Yim, D.; Kim, H. W.; Jang, W.-D.; Yoon, S. C.; Jung, I. H.; Jang, S.-Y., High-performance near-infrared absorbing n-type porphyrin acceptor for organic solar cells, *ACS Appl. Mater. Interfaces* **2018**, *10*, 41344-41349.

(17) Lewtak, J. P.; Gryko, D. T., Synthesis of π-extended porphyrins via intramolecular oxidative coupling, *Chem. Commun.* **2012**, *48*, 10069-10086.

(18) Richeter, S.; Jeandon, C.; Kyritsakas, N.; Ruppert, R.; Callot, H. J., Preparation of six isomeric bis-acylporphyrins with chromophores reaching the near-infrared via intramolecular friedel–crafts reaction, *J. Org. Chem.* **2003**, *68*, 9200-9208.

(19) Gill, H. S.; Harmjanz, M.; Santamaría, J.; Finger, I.; Scott, M. J., Facile oxidative rearrangement of dispiro-porphodimethenes to nonplanar and sheetlike porphyrins with intense absorptions in the near-ir region, *Angew. Chem. Int. Ed.* **2004**, *43*, 485-490.

(20) Kurotobi, K.; Kim, K. S.; Noh, S. B.; Kim, D.; Osuka, A., A quadruply azulene-fused porphyrin with intense near-ir absorption and a large two-photon absorption cross section, *Angew. Chem. Int. Ed.* **2006**, *45*, 3944-3947.

(21) Tokuji, S.; Takahashi, Y.; Shinmori, H.; Shinokubo, H.; Osuka, A., Synthesis of a pyridine-fused porphyrinoid: Oxopyridochlorin, *Chem. Commun.* **2009**, 1028-1030.

(22) Jiao, C.; Huang, K.-W.; Guan, Z.; Xu, Q.-H.; Wu, J., N-annulated perylene fused porphyrins with enhanced near-ir absorption and emission, *Org. Lett.* **2010**, *12*, 4046-4049.

(23) Diev, V. V.; Hanson, K.; Zimmerman, J. D.; Forrest, S. R.; Thompson, M. E., Fused pyrene–diporphyrins: Shifting near-infrared absorption to 1.5 μm and beyond, *Angew. Chem. Int. Ed.* **2010**, *49*, 5523-5526.

(24) Tanaka, T.; Osuka, A., Conjugated porphyrin arrays: Synthesis, properties and applications for functional materials, *Chem. Soc. Rev.* **2015**, *44*, 943-969.

(25) Davis, N. K. S.; Thompson, A. L.; Anderson, H. L., A porphyrin fused to four anthracenes, *J. Am. Chem. Soc.* **2011**, *133*, 30-31.

(26) Mori, H.; Tanaka, T.; Osuka, A., Fused porphyrinoids as promising near-infrared absorbing dyes, *J. Mater. Chem. C* **2013**, *1*, 2500-2519.

(27) Sun, Z.; Ye, Q.; Chi, C.; Wu, J., Low band gap polycyclic hydrocarbons: From closed-shell near infrared dyes and semiconductors to open-shell radicals, *Chem. Soc. Rev.* **2012**, *41*, 7857-7889.

(28) Shimizu, D.; Osuka, A., Porphyrinoids as a platform of stable radicals, *Chem. Sci.* **2018**, *9*, 1408-1423.

(29) Morita, Y.; Suzuki, S.; Sato, K.; Takui, T., Synthetic organic spin chemistry for structurally well-defined open-shell graphene fragments, *Nat. Chem.* **2011**, *3*, 197-204.

(30) Feringa, B. L. (ed.) *Molecular switches*; Wiley-VCH Verlag GmbH, 2001.

(31) Coronado, E.; Epsetin, A. J., Molecular spintronics and quantum computing, *J. Mater. Chem.* **2009**, *19*, 1670.

(32) Zeng, W.; Lee, S.; Son, M.; Ishida, M.; Furukawa, K.; Hu, P.; Sun, Z.; Kim, D.; Wu, J., Phenalenyl-fused porphyrins with different ground states, *Chem. Sci.* **2015**, *6*, 2427-2433.

(33) Diev, V. V.; Femia, D.; Zhong, Q.; Djurovich, P. I.; Haiges, R.; Thompson, M. E., A quinoidal bis-phenalenyl-fused porphyrin with supramolecular organization and broad near-infrared absorption, *Chem. Commun.* **2016**, *52*, 1949-1952.

(34) Umetani, M.; Naoda, K.; Tanaka, T.; Lee, S.-K.; Oh, J.; Kim, D.; Osuka, A., Synthesis of di-peri-dinaphthoporphyrins by ptcl2-mediated cyclization of quinodimethane-type porphyrins, *Angew. Chem. Int. Ed.* **2016**, *55*, 6305-6309.

(35) Ohashi, K.; Kubo, T.; Masui, T.; Yamamoto, K.; Nakasuji, K.; Takui, T.; Kai, Y.; Murata, I., 4,8,12,16-tetra-tert-butyl-s-indaceno[1,2,3-cd:5,6,7-c'd']diphenalene: A four-stage amphoteric redox system, *J. Am. Chem. Soc.* **1998**, *120*, 2018-2027.

(36) Goto, K.; Kubo, T.; Yamamoto, K.; Nakasuji, K.; Sato, K.; Shiomi, D.; Takui, T.; Kubota, M.; Kobayashi, T.; Yakusi, K.; Ouyang, J., A stable neutral hydrocarbon radical: Synthesis, crystal structure, and physical properties of 2,5,8-tri-tert-butyl-phenalenyl, *J. Am. Chem. Soc.* **1999**, *121*, 1619-1620.

(37) Kubo, T.; Sakamoto, M.; Akabane, M.; Fujiwara, Y.; Yamamoto, K.; Akita, M.; Inoue, K.; Takui, T.; Nakasuji, K., Four-stage amphoteric redox properties and biradicaloid character of tetra-tert-butyldicyclopenta[b;d]thieno[1,2,3-cd;5,6,7-c′d′]diphenalene, *Angew. Chem. Int. Ed.* **2004**, *43*, 6474-6479.

(38) Kubo, T.; Shimizu, A.; Sakamoto, M.; Uruichi, M.; Yakushi, K.; Nakano, M.; Shiomi, D.; Sato, K.; Takui, T.; Morita, Y.; Nakasuji, K., Synthesis, intermolecular interaction, and semiconductive behavior of a delocalized singlet biradical hydrocarbon, *Angew. Chem. Int. Ed.* **2005**, *44*, 6564-6568.

(39) Morita, Y.; Nishida, S. (2010). Phenalenyls, cyclopentadienyls, and other carbon-centered radicals. In *Stable radicals*; Hicks, R. G., Ed., p 81-145.

(40) Y. Gopalakrishna, T.; Zeng, W.; Lu, X.; Wu, J., From open-shell singlet diradicaloids to polyradicaloids, *Chem. Commun.* **2018**, *54*, 2186-2199.

(41) Björk, J.; Hanke, F., Towards design rules for covalent nanostructures on metal surfaces, *Chem. Eur. J.* **2014**, *20*, 928-934.

(42) Lindner, R.; Kühnle, A., On-surface reactions, *ChemPhysChem* **2015**, *16*, 1582-1592.

(43) Pavliček, N.; Schuler, B.; Collazos, S.; Moll, N.; Pérez, D.; Guitián, E.; Meyer, G.; Peña, D.; Gross, L., On-surface generation and imaging of arynes by atomic force microscopy, *Nat. Chem.* **2015**, *7*, 623.

(44) Kocić, N.; Liu, X.; Chen, S.; Decurtins, S.; Krejčí, O.; Jelínek, P.; Repp, J.; Liu, S.-X., Control of reactivity and regioselectivity for on-surface dehydrogenative aryl–aryl bond formation, *J. Am. Chem. Soc.* **2016**, *138*, 5585-5593.

(45) Held, P. A.; Fuchs, H.; Studer, A., Covalent-bond formation via on-surface chemistry, *Chem. Eur. J.* **2017**, *23*, 5874-5892.

(46) Sánchez-Sánchez, C.; Nicolaï, A.; Rossel, F.; Cai, J.; Liu, J.; Feng, X.; Müllen, K.; Ruffieux, P.; Fasel, R.; Meunier, V., On-surface cyclization of ortho-dihalotetracenes to four- and six-membered rings, *J. Am. Chem. Soc.* **2017**, *139*, 17617-17623.

(47) Pavliček, N.; Mistry, A.; Majzik, Z.; Moll, N.; Meyer, G.; Fox, D. J.; Gross, L., Synthesis and characterization of triangulene, *Nat. Nanotechnol.* **2017**, *12*, 308-311.

(48) Majzik, Z.; Pavliček, N.; Vilas-Varela, M.; Pérez, D.; Moll, N.; Guitián, E.; Meyer, G.; Peña, D.; Gross, L., Studying an antiaromatic polycyclic hydrocarbon adsorbed on different surfaces, *Nat. Commun.* **2018**, *9*, 1198.

(49) Sun, Q.; Zhang, R.; Qiu, J.; Liu, R.; Xu, W., On-surface synthesis of carbon nanostructures, *Adv. Mater.* **2018**, *30*, 1705630.

(50) Clair, S.; de Oteyza, D. G., Controlling a chemical coupling reaction on a surface: Tools and strategies for on-surface synthesis, *Chem. Rev.* **2019**, *119*, 4717-4776.

(51) Mishra, S.; Beyer, D.; Eimre, K.; Kezilebieke, S.; Berger, R.; Gröning, O.; Pignedoli, C. A.; Müllen, K.; Liljeroth, P.; Ruffieux, P.; Feng, X.; Fasel, R., Topological frustration induces unconventional magnetism in a nanographene, *Nat. Nanotechnol.* **2020**, *15*, 22-28.

(52) Li, J.; Sanz, S.; Castro-Esteban, J.; Vilas-Varela, M.; Friedrich, N.; Frederiksen, T.; Peña, D.; Pascual, J. I., Uncovering the triplet ground state of triangular graphene nanoflakes engineered with atomic precision on a metal surface, *Phys. Rev. Lett.* **2020**, *124*, 177201.

(53) Mishra, S.; Beyer, D.; Eimre, K.; Ortiz, R.; Fernández-Rossier, J.; Berger, R.; Gröning, O.; Pignedoli, C. A.; Fasel, R.; Feng, X.; Ruffieux, P., Collective all-carbon magnetism in triangulene dimers, *Angew. Chem. Int. Ed.* **2020**, *59*, 12041-12047.

(54) Su, J.; Telychko, M.; Hu, P.; Macam, G.; Mutombo, P.; Zhang, H.; Bao, Y.; Cheng, F.; Huang, Z.-Q.; Qiu, Z.; Tan, S. J. R.; Lin, H.; Jelínek, P.; Chuang, F.-C.; Wu, J.; Lu, J., Atomically precise bottom-up synthesis of π-extended [5]triangulene, *Sci. Adv.* **2019**, *5*, eaav7717.

(55) Gottfried, J. M., Surface chemistry of porphyrins and phthalocyanines, *Surf. Sci. Rep.* **2015**, *70*, 259-379.

(56) Auwärter, W.; Écija, D.; Klappenberger, F.; Barth, J. V., Porphyrins at interfaces, *Nat. Chem.* **2015**, *7*, 105-120.

(57) Wiengarten, A.; Seufert, K.; Auwärter, W.; Ecija, D.; Diller, K.; Allegretti, F.; Bischoff, F.; Fischer, S.; Duncan, D.; Papageorgiou, A.; Klappenberger, F.; Acres, R.; Ngo, T.; Barth, J., Surface-assisted dehydrogenative homocoupling of porphine molecules, *J. Am. Chem. Soc.* **2014**, *136*, 9346-9354.

(58) He, Y.; Garnica, M.; Bischoff, F.; Ducke, J.; Bocquet, M.-L.; Batzill, M.; Auwärter, W.; Barth, J. V., Fusing tetrapyrroles to graphene edges by surface-assisted covalent coupling, *Nat. Chem.* **2016**, *9*, 33.

(59) Auwärter, W.; Seufert, K.; Bischoff, F.; Ecija, D.; Vijayaraghavan, S.; Joshi, S.; Klappenberger, F.; Samudrala, N.; Barth, J. V., A surface-anchored molecular four-level conductance switch based on single proton transfer, *Nat. Nanotechnol.* **2012**, *7*, 41-46.

(60) Rubio-Verdú, C.; Sarasola, A.; Choi, D.-J.; Majzik, Z.; Ebeling, R.; Calvo, M. R.; Ugeda, M. M.; Garcia-Lekue, A.; Sánchez-Portal, D.; Pascual, J. I., Orbital-selective spin excitation of a magnetic porphyrin, *Commun. Phys.* **2018**, *1*, 15.

(61) Wiengarten, A.; Lloyd, J. A.; Seufert, K.; Reichert, J.; Auwärter, W.; Han, R.; Duncan, D. A.; Allegretti, F.; Fischer, S.; Oh, S. C.; Sağlam, Ö.; Jiang, L.; Vijayaraghavan, S.; Écija, D.; Papageorgiou, A. C.; Barth, J. V., Surface-assisted cyclodehydrogenation; break the symmetry, enhance the selectivity, *Chem. Eur. J.* **2015**, *21*, 12285-12290.

(62) Cirera, B.; de la Torre, B.; Moreno, D.; Ondráček, M.; Zbořil, R.; Miranda, R.; Jelínek, P.; Écija, D., On-surface synthesis of gold porphyrin derivatives via a cascade of chemical interactions: Planarization, self-metalation, and intermolecular coupling, *Chem. Mater.* **2019**, *31*, 3248-3256.

(63) In't Veld, M.; Iavicoli, P.; Haq, S.; Amabilino, D. B.; Raval, R., Unique intermolecular reaction of simple porphyrins at a metal surface gives covalent nanostructures, *Chem. Commun.* **2008**, 1536-1538.

(64) Grill, L.; Dyer, M.; Lafferentz, L.; Persson, M.; Peters, M. V.; Hecht, S., Nano-architectures by covalent assembly of molecular building blocks, *Nat. Nanotechnol.* **2007**, *2*, 687.

(65) Li, J.; Merino-Díez, N.; Carbonell-Sanromà, E.; Vilas-Varela, M.; de Oteyza, D. G.; Peña, D.; Corso, M.; Pascual, J. I., Survival of spin state in magnetic porphyrins contacted by graphene nanoribbons, *Sci. Adv.* **2018**, *4*, eaaq0582.

(66) Mateo, L. M.; Sun, Q.; Liu, S.-X.; Bergkamp, J. J.; Eimre, K.; Pignedoli, C. A.; Ruffieux, P.; Decurtins, S.; Bottari, G.; Fasel, R.; Torres, T., On-surface synthesis and characterization of triply fused porphyrin–graphene nanoribbon hybrids, *Angew. Chem. Int. Ed.* **2020**, *59*, 1334-1339.

(67) van Vörden, D.; Lange, M.; Schmuck, M.; Schaffert, J.; Cottin, M. C.; Bobisch, C. A.; Möller, R., Communication: Substrate induced dehydrogenation: Transformation of octa-ethyl-porphyrin into tetra-benzo-porphyrin, *J. Chem. Phys.* **2013**, *138*, 211102.

(68) Treier, M.; Pignedoli, C. A.; Laino, T.; Rieger, R.; Müllen, K.; Passerone, D.; Fasel, R., Surface-assisted cyclodehydrogenation provides a synthetic route towards easily processable and chemically tailored nanographenes, *Nat. Chem.* **2010**, *3*, 61.

(69) Lindsey, J. S.; Schreiman, I. C.; Hsu, H. C.; Kearney, P. C.; Marguerettaz, A. M., Rothemund and adler-longo reactions revisited: Synthesis of tetraphenylporphyrins under equilibrium conditions, *J. Org. Chem.* **1987**, *52*, 827-836.

(70) Kruszewski, J.; Krygowski, T. M., Definition of aromaticity basing on the harmonic oscillator model, *Tetrahedron Lett.* **1972**, *13*, 3839-3842.

(71) Matito, E.; Poater, J.; Solá, M. (2007). Aromaticity analysis by means of the quantum theory of atoms in molecules. In *The quantum theory of atoms in molecules*; Matta, C. F., Boyd, R. J., Eds., p 399-423.

(72) Ternes, M., Spin excitations and correlations in scanning tunneling spectroscopy, *New Journal of Physics* **2015**, *17*, 063016.

(73) Ternes, M.; Heinrich, A. J.; Schneider, W.-D., Spectroscopic manifestations of the kondo effect on single adatoms, *J. Phys.: Condens. Matter* **2008**, *21*, 053001.

(74) Li, J.; Sanz, S.; Corso, M.; Choi, D. J.; Peña, D.; Frederiksen, T.; Pascual, J. I., Single spin localization and manipulation in graphene open-shell nanostructures, *Nat. Commun.* **2019**, *10*, 200.

(75) Mugarza, A.; Krull, C.; Robles, R.; Stepanow, S.; Ceballos, G.; Gambardella, P., Spin coupling and relaxation inside molecule–metal contacts, *Nat. Commun.* **2011**, *2*, 490.

(76) Gross, L.; Moll, N.; Mohn, F.; Curioni, A.; Meyer, G.; Hanke, F.; Persson, M., High-resolution molecular orbital imaging using a *p*-wave stm tip, *Phys. Rev. Lett.* **2011**, *107*, 086101.

(77) Mielke, J.; Hanke, F.; Peters, M. V.; Hecht, S.; Persson, M.; Grill, L., Adatoms underneath single porphyrin molecules on au(111), *J. Am. Chem. Soc.* **2015**, *137*, 1844-1849.

(78) Kumar, A.; Banerjee, K.; Dvorak, M.; Schulz, F.; Harju, A.; Rinke, P.; Liljeroth, P., Charge-transfer-driven nonplanar adsorption of f4tcnq molecules on epitaxial graphene, *ACS Nano* **2017**, *11*, 4960-4968.

(79) Zhao Yan; Jiang Kaiyue; Li Can; Liu Yufeng; Xu Chengyang; Zheng Wenna; Guan Dandan; Li Yaoyi; Zheng Hao; Liu Canhua; Luo Weidong; Jia Jinfeng; Zhuang Xiaodong; Shiyong, W., Precise control of π-electron magnetism in nonmetal porphyrins, *ChemRxiv* **2020**.

Table of Contents (ToC)